and to the further development of the methods employed in the theory of nuclear matter in order to treat the varying density and finite geometry of nuclei. It may be expected that this development will lead to important insight into many nuclear properties, such as the various components in the nuclear optical potential, the effective interactions in the nucleus, and the structure of the nuclear surface. However, the development is still in a preliminary stage, and we have not attempted to include a systematic treatment of the formalism in the present text.

ILLUSTRATIVE EXAMPLES TO SECTION 2-5

Phase shift analysis for nucleon-nucleon scattering (Fig. 2-34)

The scattering amplitude for two spin one-half particles is a 4×4 matrix in the spin variables, as well as a function of the energy E and scattering angles ϑ, φ. Since the nucleon-nucleon interaction commutes with the total spin S as well as with the parity π and the total angular momentum J (see p. 68), it is convenient to expand the scattering matrix in terms of channels labeled by these quantum numbers. The channels with $S = 0$ ($J = L$, $\pi = (-1)^L$) and $S = 1$, $J = L$ ($\pi = (-1)^L$) are uncoupled and thus the scattering matrix is described by a single real parameter, the phase shift δ. The centrifugal barrier implies that, at low energies ($ka \ll L^{1/2}$, where a is a measure of the range of interaction), the phase shift $\delta(L)$ is proportional to k^{2L+1} (see, for example, Eq. (3F-37) and Table 3F-1). In the present analysis, we shall neglect the possibility of inelastic reactions, which may occur for energies above the threshold for meson production ($E_{\text{Lab}} > 280$ MeV); in practice, the meson production cross sections near threshold are sufficiently small so that the elastic scattering amplitudes remain approximately unitary up to laboratory energies of about 400 MeV (see, for example, Hama and Hoshizaki, 1964, and Azhgirey *et al.*, 1963).

The channels $S = 1$, $L = J - 1$ and $S = 1$, $L = J + 1$ are coupled by the tensor force and thus the scattering amplitude is a 2×2 matrix in these channels. A unitary 2×2 matrix requires three independent parameters. The analysis shown in Fig. 2-34 employs two real phase shifts ($\delta(L = J - 1, J)$, $\delta(L = J + 1, J)$) and a real mixing parameter ε_J. In terms of these parameters, the S matrix is

$$S^{(J)} = \begin{pmatrix} \exp\{i\delta(L = J-1, J)\} & 0 \\ 0 & \exp\{i\delta(L = J+1, J)\} \end{pmatrix} \begin{pmatrix} \cos 2\varepsilon_J & i \sin 2\varepsilon_J \\ i \sin 2\varepsilon_J & \cos 2\varepsilon_J \end{pmatrix} \times \begin{pmatrix} \exp\{i\delta(L = J-1, J)\} & 0 \\ 0 & \exp\{i\delta(L = J+1, J)\} \end{pmatrix} \tag{2-222}$$

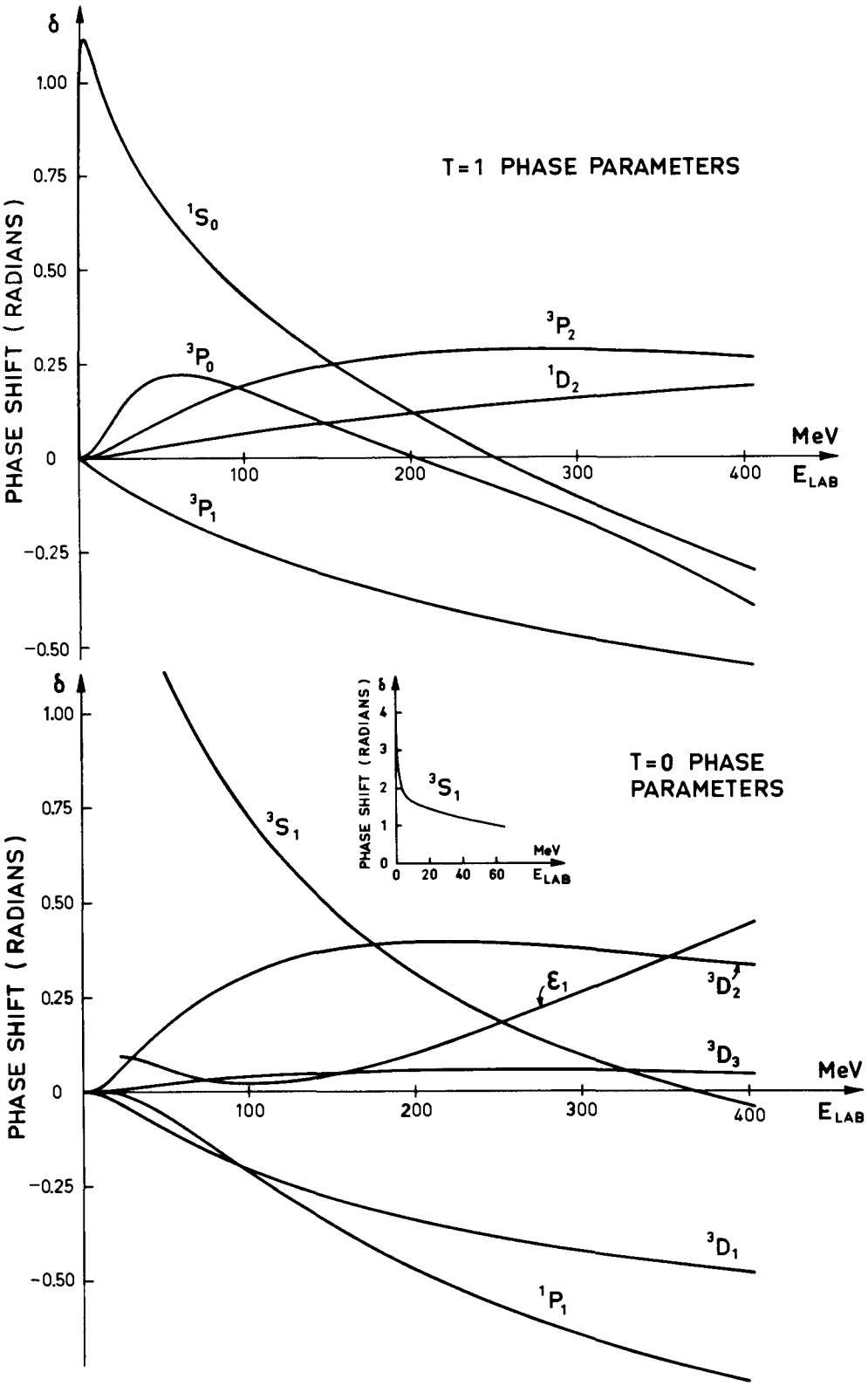
δ
1.00
0.75
0.50
0.25
0
−0.25
−0.50
PHASE SHIFT (RADIANS)
T=1 PHASE PARAMETERS
$^1S_0$
$^3P_2$
$^3P_0$
$^1D_2$
$^3P_1$
100
200
300
400
MeV
E_{LAB}
δ
1.00
0.75
0.50
0.25
0
−0.25
−0.50
PHASE SHIFT (RADIANS)
$^3S_1$
T=0 PHASE PARAMETERS
$^3S_1$
ε_1
$^3D_2$
$^3D_3$
$^3D_1$
$^1P_1$
100
200
300
400
MeV
E_{LAB}
δ
4
3
2
1
0
PHASE SHIFT (RADIANS)
$^3S_1$
0
20
40
60
MeV
E_{LAB}

264 圖

▼ This parameterization was introduced by Stapp *et al.* (1957), and is often referred to as the "nuclear bar" phase shifts. At low energies, $\varepsilon_J \approx$ const k^{2J}, $\delta(L, J) \approx$ const k^{2L+1}. In general, each of the phases $\delta(L = J - 1, J)$ and $\delta(L = J + 1, J)$ describes scattering involving both $L = J \pm 1$; only in the limit $E \to 0$, where $\varepsilon_J \to 0$, does the quantum number L have a simple significance for the wave function of the scattered particle.

The phase parameters shown in Fig. 2-34 are obtained from an analysis involving a large variety of different experimental data taken at many different energies. The phases are expanded in terms of assumed energy-dependent functions, which are chosen so that the contribution of the one-pion exchange potential (2-190) dominates at sufficiently low energies (except for the S and P wave channels). The coefficients of the energy-dependent functions are then varied to fit the experimental data; 58 adjustable parameters were employed in the analysis, which utilized 704 different pieces of experimental data. The phases fit the experimental data with a sum squared error of $\chi^2 = 646$.

The phase parameters in Fig. 2-34 describe the scattering due to the nuclear forces; to obtain the experimentally measured scattering amplitude, one must add the Coulomb phase shifts in the case of *pp* scattering.

Phenomenological nucleon-nucleon potentials (Fig. 2-35; Tables 2-3, 2-4)

The nucleon-nucleon potentials shown in Fig. 2-35 are parametrized in terms of the following functions:

$$
\begin{aligned}
V &= V_C(r) + V_T(r)S_{12} + V_{LS}(r)\mathbf{L}\cdot\mathbf{S} + V_{LL}(r)L_{12} \\
S_{12} &= \frac{3}{r^2}(\boldsymbol{\sigma}_1\cdot\mathbf{r})(\boldsymbol{\sigma}_2\cdot\mathbf{r}) - \boldsymbol{\sigma}_1\cdot\boldsymbol{\sigma}_2 \\
L_{12} &= (\boldsymbol{\sigma}_1\cdot\boldsymbol{\sigma}_2)\mathbf{L}^2 - \tfrac{1}{2}[(\boldsymbol{\sigma}_1\cdot\mathbf{L})(\boldsymbol{\sigma}_2\cdot\mathbf{L}) + (\boldsymbol{\sigma}_2\cdot\mathbf{L})(\boldsymbol{\sigma}_1\cdot\mathbf{L})] \\
&= (\delta_{LJ} + \boldsymbol{\sigma}_1\cdot\boldsymbol{\sigma}_2)\mathbf{L}^2 - (\mathbf{L}\cdot\mathbf{S})^2
\end{aligned}
\qquad (2\text{-}223)
$$

and thus contain central (V_C), tensor (V_T), spin-orbit (V_{LS}), and second-order spin-orbit (V_{LL}) components. The radial functions are restricted by the condition ▲ that, at large distances, the central and tensor potentials should be described by

---

Figure 2-34 The figure illustrates the phase parameters for nucleon-nucleon scattering in the channels with $L \leq 2$. The low-energy behavior is determined by the effective range parameters (2-183); the data for $E > 24$ MeV are taken from the analysis by R. A. Arndt and M. H. MacGregor, *Phys. Rev.* **141**, 873 (1966); similar analyses have been given by Breit *et al.* (1962), Hull *et al.* (1962), and, more recently, by MacGregor *et al.* (1968). The definition of the phase parameters in terms of the scattering matrix is given by Eq. (2-222).

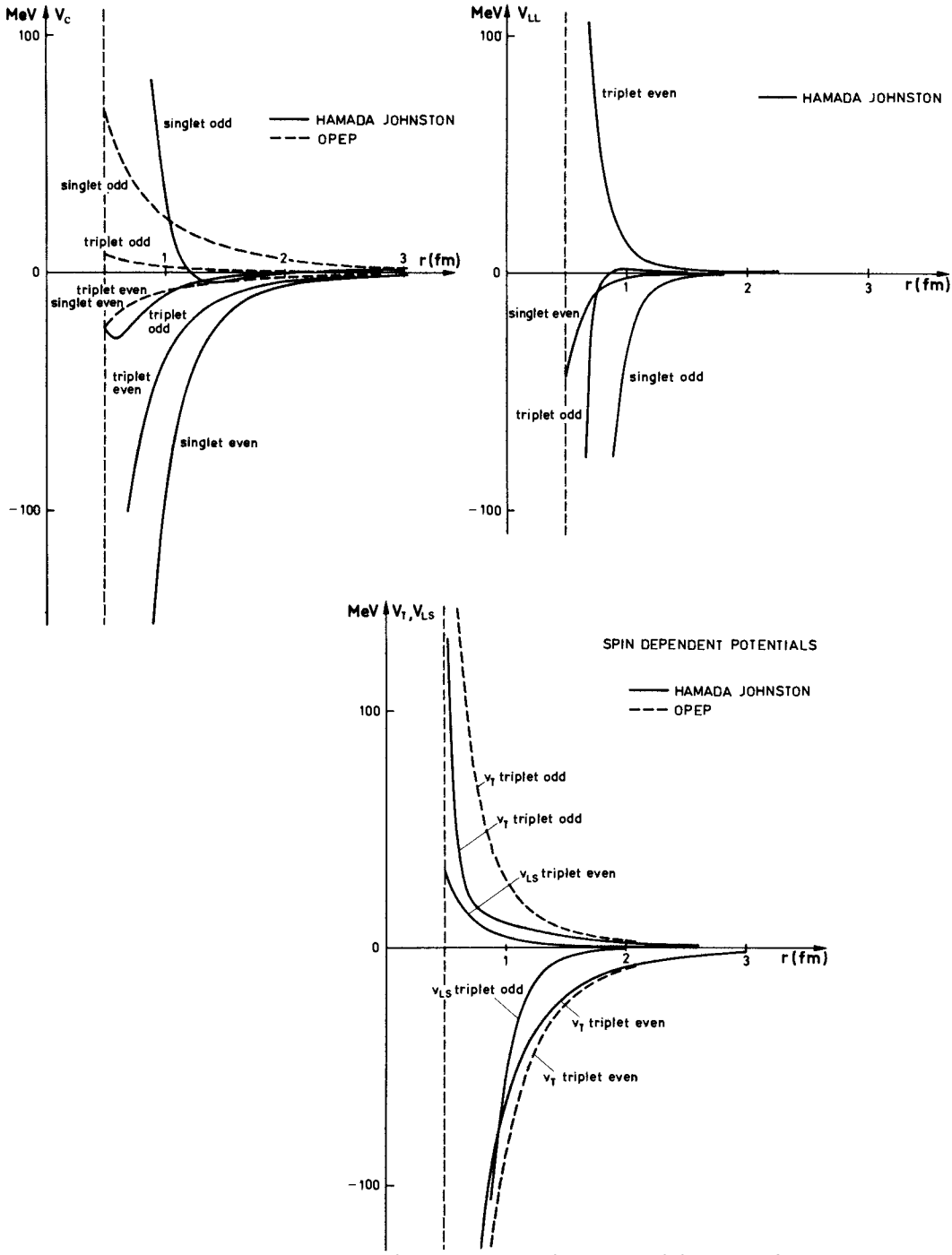

Figure 2-35 The phenomenological nucleon-nucleon potentials shown in the figure are taken from the analysis of T. Hamada and I. D. Johnston, *Nuclear Phys.* 34, 382 (1962); similar potentials have been obtained by Lassila *et al.* (1962). The dotted potentials (OPEP) correspond to the one-pion exchange potential (Eq. (2-190)). For an example of a soft-core potential, see Reid (1968), and for a nonlocal potential, see Tabakin (1964).

▼ the one-pion exchange interaction (2-190). The assumed radial forms are

$$
\begin{aligned}
V_C &= v_0(\tau_1 \cdot \tau_2)(\sigma_1 \cdot \sigma_2)\, Y(x)[1 + a_C Y(x) + b_C Y^2(x)] \\
V_T &= v_0(\tau_1 \cdot \tau_2)(\sigma_1 \cdot \sigma_2) Z(x)[1 + a_T\, Y(x) + b_T\, Y^2(x)] \\
V_{LS} &= g_{LS} v_0\, Y^2(x)[1 + b_{LS}\, Y(x)] \\
V_{LL} &= g_{LL} v_0 \frac{Z(x)}{x^2}\,[1 + a_{LL}\, Y(x) + b_{LL}\, Y^2(x)] \\
v_0 &= \frac{1}{3}\frac{f^2}{\hbar c} m_\pi c^2 = 3.65 \text{ MeV} \\
x &= \frac{m_\pi c}{\hbar} r = \left(\frac{r}{1.43 \text{ fm}}\right) \\
Y(x) &= \frac{1}{x}\exp\{-x\} \\
Z(x) &= \left(1 + \frac{3}{x} + \frac{3}{x^2}\right) Y(x)
\end{aligned}
\qquad (2\text{-}224)
$$

and, in addition, the potential has been assumed to contain a component giving rise to infinite repulsion at the radius

$$c = 0.49 \text{ fm} \qquad (x_c = 0.343) \qquad (2\text{-}225)$$

The optimum adjustment of the 29 parameters in the above functions yields the parameter values given in Table 2-3 and the potentials shown in Fig. 2-35. The values of the different potential components at the hard-core ▲ radius, c, are listed in Table 2-4.

	Singlet even	Triplet even	Singlet odd	Triplet odd
a_C	8.7	6.0	−8.0	−9.07
b_C	10.6	−1.0	12.0	3.48
a_T	—	−0.5	—	−1.29
b_T	—	0.2	—	0.55
g_{LS}	—	2.77	—	7.36
b_{LS}	—	−0.1	—	−7.1
g_{LL}	−0.033	0.10	−0.10	−0.033
a_{LL}	0.2	1.8	2.0	−7.3
b_{LL}	−0.2	−0.4	6.0	6.9

Table 2-3 Parameters of the Hamada-Johnston potential illustrated in Fig. 2-35.

▼ It should be emphasized that the fit to the experimental data obtained with the potential of Fig. 2-35 is appreciably poorer than the fit with the phase param- ▲ eters given in Fig. 2-34, and thus there remains some uncertainty concerning

▼ the correct form of the nucleonic interaction. (For a discussion of the goodness
▲ of fit of the potential models, see Amati, 1964.)

	Potentials (MeV)			
	V_C	V_T	V_{LS}	V_{LL}
Singlet even	−1460	–	–	−42
Triplet even	−207	−642	34	668
Singlet odd	2371	–	–	−6683
Triplet odd	−23	173	−1570	−1087

Table 2-4 Values of the Hamada-Johnston potential at $r = c = 0.49$ fm (see Table 2-3.)

▼ In Fig. 2-35, the one-pion exchange potentials (2-190) are also drawn. These components represent the main part of the nucleonic interaction for $r \gtrsim 3$ fm.

Comparison between atomic and nuclear binding forces (Fig. 2-36)

It is instructive to compare the nuclear two-body forces with those acting in the diatomic molecule H_2 (see Fig. 2-36). An appropriate unit of energy for such a comparison is $\hbar^2/Mc^2$, where c is the extension of the repulsive short-range potential. For molecules, c is of the order of the atomic radius $a \sim \hbar^2/e^2m$, where m is the electron mass; more precisely, we choose c to be the distance at which the potential vanishes. Figure 2-36 also shows the radial density distribution, $\varphi^2 = (r\mathcal{R}(r))^2$, for the lowest bound states.

The chemical forces between the atoms are determined by the electronic structure, and the strength of the potential is thus

$$V_{\text{mol}} \sim \frac{e^2}{a} \sim \frac{\hbar^2}{ma^2} \tag{2-226}$$

which is of order M/m on the scale considered. Such a very strong binding potential implies that the ground state wave function is strongly peaked at the minimum of the potential, and the binding energy is large compared with the zero-point kinetic energy; such a system possesses a vibrational-rotational spectrum. When more particles are added, one obtains a closely packed system with a density $\approx c^{-3}$. At low temperatures, such systems usually crystallize. (An exception is He, where the forces are relatively weak and the density relatively low; see de Boer, 1957, for a comparison of the properties of condensed systems as a function of the dimensionless interaction parameter $(Mc^2\hbar^{-2})$.)

The nuclear forces are relatively weak. The attraction close to the core, which is of order unity on the scale considered, is not sufficient to produce a
▲ bound state; the deuteron state only arises as a consequence of the tail of the